

Large impact of coarse-resolution atmospheric transport model error on land-ocean and tropic-extratropic partitioning and seasonal cycle in CO₂ inversion

Zhiqiang Liu¹, Ning Zeng², Pengfei Han³, and Qixiang Cai³

¹Institute of Atmospheric Physics

²University of Maryland, College Park

³Institute of Atmospheric Physics, Chinese Academy of Sciences

April 16, 2023

Abstract

We show that forward simulations of global CO₂ using an atmospheric transport model (ATM) at $0.5^\circ \times 0.625^\circ$ and $4^\circ \times 5^\circ$ resolutions differ significantly in vertical and meridional distribution. Comparing two observing simulation system experiments at $4^\circ \times 5^\circ$ resolution that assimilate pseudo observations sampled from the two forward simulations, we isolated the impact of coarse-resolution ATM error on regional flux estimates that a significant amount of annual carbon uptake from the ocean and tropics is improperly redistributed to the land and extratropics, respectively. In addition, this error leads to an underestimated seasonal amplitude in the northern extratropical land and a reversed seasonal phase in the northern extratropical ocean. The reversed seasonal phase has also been shown in a real data assimilation experiment and state-of-the-art inversions, suggesting that ocean glint retrieval error may not be as significant as previously thought and reasonable ocean flux estimates depend strongly on the accuracy of ATM.

1 **Large impact of coarse-resolution atmospheric transport model error on land-ocean**
2 **and tropic-extratropic partitioning and seasonal cycle in CO₂ inversion**
3

4 **Zhiqiang Liu^{1,2}, Ning Zeng^{3,4}, Pengfei Han^{5,1}, Qixiang Cai¹**

5 ¹Laboratory of Numerical Modeling for Atmospheric Sciences & Geophysical Fluid Dynamics,
6 Institute of Atmospheric Physics, Chinese Academy of Sciences, Beijing, China

7 ²University of Chinese Academy of Sciences, Beijing, China

8 ³Dept. of Atmospheric and Oceanic Science, University of Maryland, USA

9 ⁴Earth System Science Interdisciplinary Center, University of Maryland, USA

10 ⁵Carbon Neutrality Research Center, Institute of Atmospheric Physics, Chinese Academy of
11 Sciences, Beijing, China

12 Corresponding authors: Zhiqiang Liu (liuzhiqiang@mail.iap.ac.cn)

13 **Key Points:**

- 14 ● Error from the coarse-resolution atmospheric transport model can introduce systematic
15 biases to CO₂ modeling and inversed flux estimates.
- 16 ● The coarse-resolution transport error leads to stronger land and extratropical sink
17 estimates and weaker ocean and tropical sink estimates.
- 18 ● The error also induces an underestimated seasonal amplitude and a reversed seasonal
19 phase in the northern land and ocean, respectively.

20 **Abstract**

21 We show that forward simulations of global CO₂ using an atmospheric transport model (ATM) at
22 0.5° × 0.625° and 4° × 5° resolutions differ significantly in vertical and meridional distribution.
23 Comparing two observing simulation system experiments at 4° × 5° resolution that assimilate
24 pseudo observations sampled from the two forward simulations, we isolated the impact of
25 coarse-resolution ATM error on regional flux estimates that a significant amount of annual
26 carbon uptake from the ocean and tropics is improperly redistributed to the land and extratropics,
27 respectively. In addition, this error leads to an underestimated seasonal amplitude in the northern
28 extratropical land and a reversed seasonal phase in the northern extratropical ocean. The reversed
29 seasonal phase has also been shown in a real data assimilation experiment and state-of-the-art
30 inversions, suggesting that ocean glint retrieval error may not be as significant as previously
31 thought and reasonable ocean flux estimates depend strongly on the accuracy of ATM.

32 **Plain Language Summary**

33 Credible regional carbon budget estimates from atmospheric CO₂ measurements rely on the
34 accuracy of atmospheric transport models (ATMs). However, the simulated atmospheric vertical
35 motions in ATMs are usually simplified and spatiotemporally averaged, leading to systematic
36 biases in simulating the long-lived atmospheric CO₂ and estimating surface carbon fluxes. Even
37 though the atmospheric approach is increasingly applied to account for country-level carbon
38 budget in global synthesis activities. Our finding suggests that current coarse-resolution ATMs
39 lead to improper attribution of annual carbon uptake from the ocean and tropics to the land and
40 extratropics, respectively, resulting in overestimated natural carbon uptake and reduced
41 emissions reduction duty in most advanced countries that target carbon neutrality. Furthermore,
42 since the seasonal variation of carbon flux in the ocean is much smaller than in the land, the
43 results indicate that a small seasonal bias from the land can overwrite and even reverse the real
44 flux signal in the ocean.

45 **1 Introduction**

46 Quantifying the country-level CO₂ budget using atmospheric CO₂ inversion technique is
47 one of the critical approaches in the upcoming Global StockTake assessment (Chevallier, 2021;
48 Jiang et al., 2022; Weir et al., 2022; Deng et al., 2022; Byrne et al., 2023). However, several
49 fundamental issues in CO₂ inversion (e.g., transport, satellite retrieval, and a priori errors) have
50 not been fully addressed, challenging the derivation of robust regional CO₂ budget estimation
51 (Fu et al., 2021; O'Dell et al., 2018; Philip et al., 2019; Schuh et al., 2019). Inversion systems
52 use an offline atmosphere transport model (ATM) to relate the surface land and ocean carbon
53 fluxes with observed CO₂ concentration. An offline ATM is driven by the meteorology
54 reanalysis data generated from a general circulation model (GCM), which significantly reduces
55 the computational cost but simplifies and spatiotemporally averages some nonlinear atmospheric
56 processes (J. Liu et al., 2011; Basu et al., 2018; Schuh et al., 2019). The averaging processes
57 include remapping the GCM output from seconds to hours and irregular grid to latitude-
58 longitude grid, and spatial interpolation from native to coarse horizontal resolution, which
59 induces underestimated transient vertical motion and reduced vertical transport (Yu et al., 2018).
60 Recent forward modeling studies find that the simulated CO₂ concentrations are significantly
61 different in vertical and meridional distribution using different ATM configurations and ATMs
62 (Schuh et al., 2019; Schuh & Jacobson, 2022). These biases can influence the estimates of

63 regional carbon budgets (Wang et al., 2020; Schuh et al., 2022) and seasonal cycles (Cui et al.,
64 2022) estimates. A large discrepancy between the inversion estimates and process
65 understandings is the land-ocean and tropic-extratropic partitioning of carbon fluxes. The
66 inversions usually estimate a large carbon sink in the northern extratropics and a weak carbon
67 sink or carbon source in the tropics recently, while process models or inventories suggest more
68 carbon uptake in the tropics (Schimel et al., 2015; Friedlingstein et al., 2022). Evidence from the
69 vertical CO₂ observation profiles indicates that inversions may overestimate the northern sink
70 and underestimate the tropical sink (Stephens et al., 2007).

71 To reduce the main transport error, running global inversions at the native resolution is a
72 straightforward strategy. However, native resolution inversions can be very slow due to reading
73 and writing a large amount of data and poor parallel methods in some ATMs (e.g., classic
74 GEOS-Chem) (The International GEOS-Chem User Community, 2021). For example, forward
75 simulation of global CO₂ at a native horizontal resolution of $0.5^\circ \times 0.625^\circ$ using GEOS-Chem
76 requires around 60 gigabytes (GB) of memory and could be paralleled using OpenMP only that a
77 one-year simulation costs more than 1 week using 1 Central Processing Unit (CPU) with 20
78 cores. The computation costs will increase dramatically by at least an order of magnitude when
79 conducting ensemble or adjoint simulation, thus not possible in real inversion applications but
80 acceptable in simple forward simulation. In this study, instead of conducting native inversion
81 directly, we, for the first time, derived the impact of coarse resolution transport model error on
82 large-scale flux distribution in the context of observing simulation system experiments (OSSEs)
83 and further suggested that the estimated northern ocean fluxes in current state-of-the-art
84 inversion systems are likely driven by the transport error instead of observation information or
85 satellite retrieval errors. Section 2 describes the data and method; Section 3 shows the results; the
86 conclusion and discussion are presented in the last section.

87 **2 Data and method**

88 We use the Carbon in Ocean-Land-Atmosphere (COLA) system (Z. Liu et al., 2022,
89 2023) to understand the transport impact on flux estimation in the context of Observing
90 Simulation System Experiments (OSSEs) and a real data assimilation experiment. COLA
91 optimizes the land (F_{TA}) and ocean (F_{OA}) carbon fluxes using a local ensemble transform Kalman
92 filter and a constrained ensemble Kalman filter, while terrestrial fire flux (F_{IR}) and anthropogenic
93 fossil fuel emissions (F_{FE}) are not optimized. The atmosphere transport model used in COLA is
94 GEOS-Chem of version 13.0.2, driven by the Modern-Era Retrospective analysis for Research
95 and Applications Version 2 (MERRA-2) meteorology reanalysis (Gelaro et al., 2017; The
96 International GEOS-Chem User Community, 2021). The native spatial resolution of MERRA-2
97 is $0.5^\circ \times 0.625^\circ$.

98 In this study, two sets of OSSEs are performed from December 2014 to the end of 2015.
99 In the first OSSE (EXP-biased), the assimilation run is conducted at $4^\circ \times 5^\circ$ resolution while the
100 nature run is conducted at the native $0.5^\circ \times 0.625^\circ$ resolution. In the second OSSE (EXP-perfect),
101 both the assimilation run and nature run are conducted at $4^\circ \times 5^\circ$ resolution. The pseudo surface
102 and satellite observation network are almost identical to Liu et al. (2022) but with additional
103 ocean glint observations from the Orbiting Carbon Observatory-2 (OCO-2) (O'Dell et al., 2018;
104 Baker et al., 2022). This kind of observation network was usually called LNLGOGIS in the
105 OCO-2 flux model intercomparison project (OCO2MIP) (Crowell et al., 2019; Peiro et al., 2022;
106 Byrne et al., 2023). Then the pseudo observations in each OSSE are sampled from their

107 corresponding nature runs and randomly perturbed based on the error scales described in Liu et
108 al. (2022). The nature runs start from the same initial CO₂ concentration and are forced by
109 identical surface carbon fluxes with the F_{FE} from the Open-source Data Inventory of
110 Anthropogenic CO₂ emissions (ODIAC) (Oda et al., 2018), the F_{IR} from Global Fire
111 Assimilation System (GFAS) (Kaiser et al., 2012), the F_{OA} from Rödenbeck et al. (2014), and the
112 F_{TA} generated from the terrestrial model of Simple Biosphere Model Version 4 (SiB4) (Haynes
113 et al., 2019). To separate the impact of model resolution while with less impact from a priori
114 fluxes, the a priori F_{TA} and F_{OA} used in the assimilation runs are similar as in the nature runs but
115 from 4 years ago.

116 In addition to the two OSSEs, a real data assimilation experiment (EXP-real) is
117 conducted at 4° × 5° resolution that assimilates the LNLGOGIS observations. And the a priori
118 fluxes and assimilation period are identical to the nature run of EXP-biased. An ensemble of
119 global inversion results (Ames, Baker, CSU, CT, OU, and TM5-4DVAR) within version 10 of
120 OCO2MIP that assimilate the LNLGOGIS observations and without very tight ocean a priori
121 constraint is used to validate the transport bias impact further (Byrne et al., 2023). Moreover, 4 a
122 priori of "bottom-up" ocean flux products in the OCO2MIP systems are used as references.

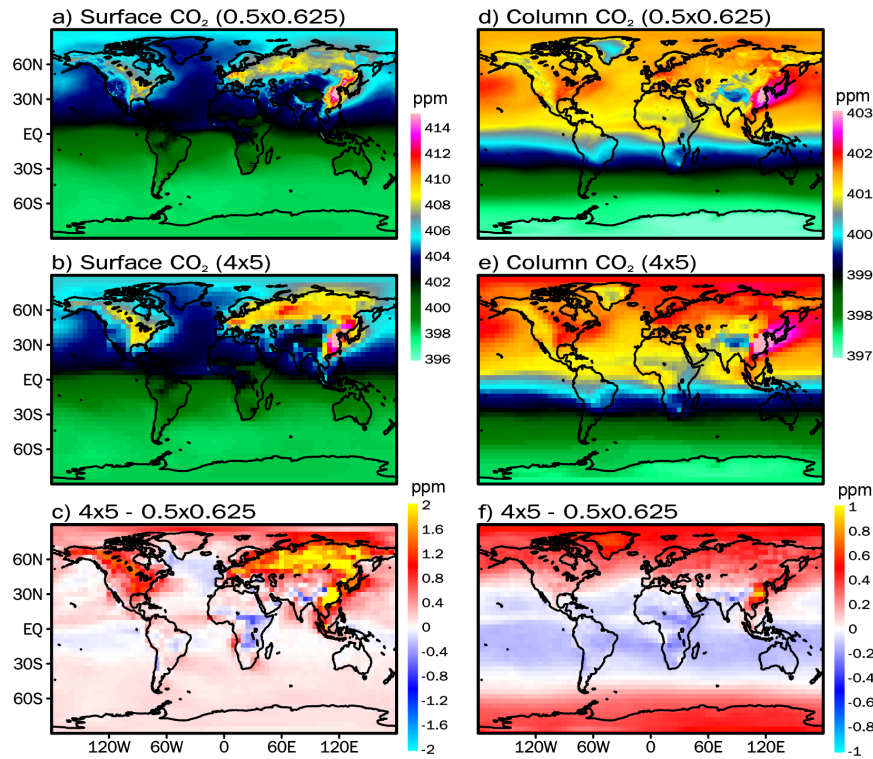
123 **3 Results**

124 **3.1 Land-ocean and tropic-extratropic partitioning**

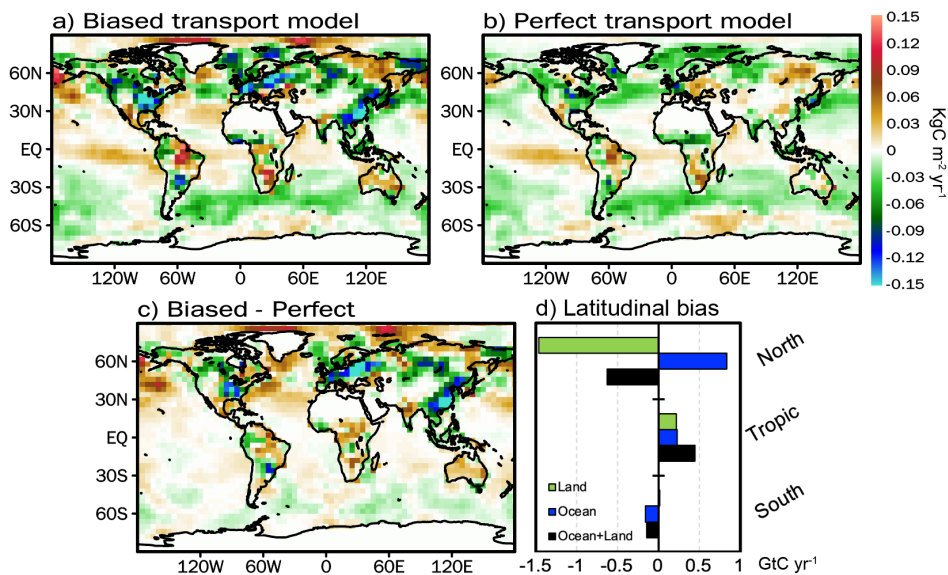
125 First, we analyze the surface CO₂ and column CO₂ (XCO₂) concentration in the nature
126 runs of EXP-bias (Figure 1a, d) and EXP-perfect (Figure 1b, e). Even though the two nature runs
127 are driven by the same surface fluxes (Figure S1), the biased ATM at 4° × 5° resolution tends to
128 trap the CO₂ fluxes within the near-surface in the Northern Hemisphere than the ATM at native
129 0.5° × 0.625° resolution on an annual average basis, especially in Eurasia that the biases can
130 reach to over 2 ppm. The XCO₂ bias has clear latitudinal distribution with positive bias in the
131 Northern (30°N~ 90°N) and Southern (-90°S~ -30°S) middle and high latitudes and negative
132 bias near the tropics (-30°S~ 30°N). Moreover, the annual bias is averaged from the seasonal
133 varying biases. In Eurasia, the positive surface bias of over 5 ppm from January to March is
134 reversed to the negative surface bias of over -3 ppm from July to September (Figure S2, S3). The
135 seasonal variation of XCO₂ bias is relatively smaller than the surface CO₂. The persistent dipole
136 tropic versus extratropic bias pattern moves southward from winter to summer.

137 The systematic error of simulated CO₂ concentration caused by the coarse-resolution
138 ATM is expected to cause significant bias in flux estimates. The first assimilation run of EXP-
139 biased assimilates the "perfect" observations but uses the "biased" ATM, which is similar to the
140 real-world scenario. Instead, the second assimilation run of EXP-perfect has no transport model
141 error issue that assimilates the "perfect" observations and uses the "perfect" ATM. The
142 difference in estimated fluxes between the two assimilation runs is expected to be the impact of
143 transport error on flux estimation. Annually, the absolute value of regional land fluxes in EXP-
144 biased is significantly larger than EXP-perfect (Figure 2a, b). In the northern mid-latitudes land
145 area, the carbon sink is largely overestimated in EXP-biased, especially in eastern China, eastern
146 North America, and Europe. About half of this sink is compensated by the surrounding
147 weakened ocean sink and carbon release in the high latitude of East Siberia (Figure 2d). Moving
148 southward, EXP-biased shows less carbon sink in the tropical ocean, South America, Australia,
149 and Africa and more carbon sink in the Southern Ocean. Generally, relative to EXP-perfect, the

150 transport error tends to enhance the land carbon sink by 1.23 GtC yr⁻¹ and weaken the ocean
 151 carbon sink by 0.9 GtC yr⁻¹. Moreover, more carbon sink of 0.77 GtC yr⁻¹ is attributed to the
 152 extratropics (-90 °S~ -23 °S and 23 °N~ 90 °N), and 0.44 GtC yr⁻¹ more carbon is released from
 153 the tropics (-23 °S~ 23 °N), resulting in a global net flux bias of -0.33 GtC yr⁻¹. Due to the high
 154 computation and memory cost, we only conduct tests for 1 year. Further research on how ATM
 155 bias affects interannual flux estimation is worth investigating in the future.



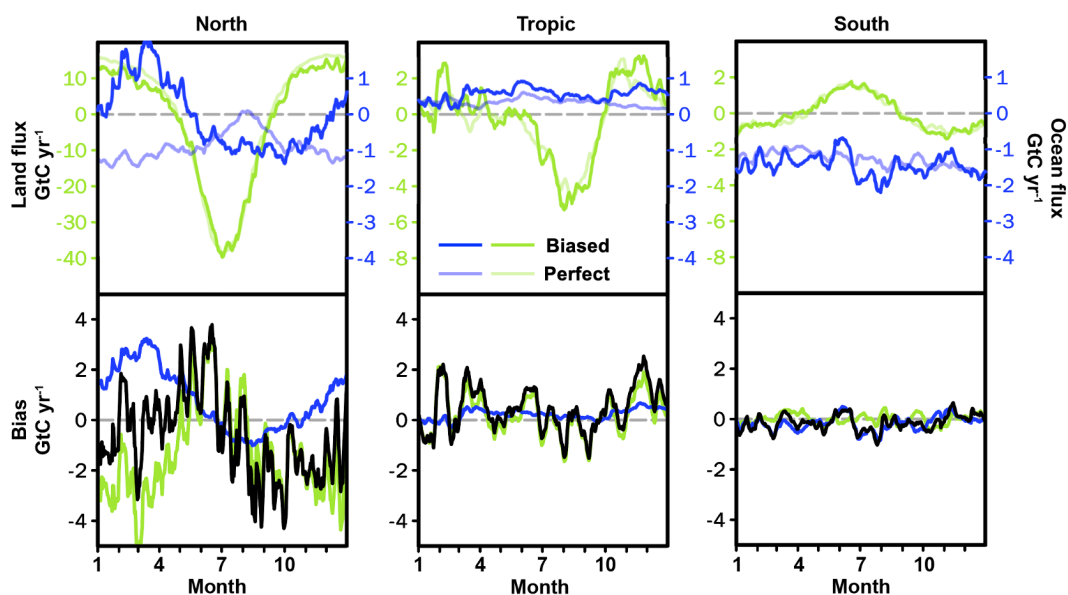
156 **Figure 1. The annual mean surface CO₂ and column CO₂ pattern of nature runs at**
 157 **horizontal resolutions of 0.5° × 0.625° (a, d) and 4° × 5° (b, e). (c, f) The difference between**
 158 **the two nature runs.**
 159



161 **Figure 2. The spatial pattern of optimized annual mean land and ocean fluxes of**
 162 **assimilation runs of EXP-biased (a) and EXP-perfect (b). (c) The difference between the**
 163 **two assimilation runs. (d) The difference in land and ocean fluxes between the two**
 164 **assimilation runs in latitude bands of northern extratropics (23 °N ~ 90 °N), tropics (-23 °S**
 165 **~ 23 °N), and southern extratropics (-90 °S ~ -23 °S).**

166 3.2 Seasonal cycle

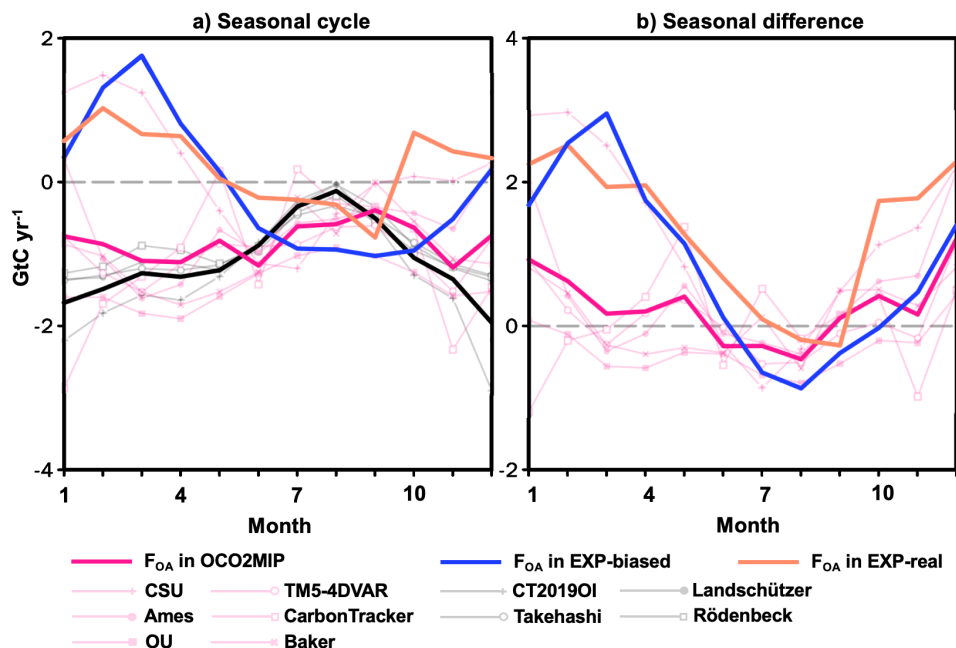
167 At the seasonal scale, the seasonal amplitude of the northern extratropical land flux is
 168 significantly underestimated in EXP-biased, mainly due to less carbon release during the non-
 169 growing seasons (Figure 3). In the northern extratropical ocean, the seasonal phase is reversed
 170 and the seasonal strength is enhanced, which partly compensates for the weakened seasonal
 171 amplitude in the northern extratropical land. The seasonal biases are smaller in the tropics and
 172 southern extratropics. From January to May, a large amount of carbon is released from the
 173 northern ocean. And the relative impact of transport error on the ocean flux is significantly larger
 174 than the land flux, implying that the ocean flux estimation in the context of the transport error
 175 may not be better than those a priori estimations. To overcome this limitation, inverse modelers
 176 usually apply tight a priori constraints on ocean flux in the real-world scenario (Peylin et al.,
 177 2013).



178 **Figure 3. The upper figures are the seasonal cycle of land (green) and ocean (blue) fluxes**
 179 **of EXP-biased (darker color) and EXP-perfect (lighter color) at daily timestep in latitude**
 180 **bands of northern extratropics (23 °N ~ 90 °N), tropics (-23 °S ~ 23 °N), and southern**
 181 **extratropics (-90 °S ~ -23 °S). The bottom figures are the land, ocean, and net (black) fluxes**
 182 **difference between EXP-biased and EXP-perfect.**

184 Global inversion systems were usually run at a coarse horizontal resolution of 2° to 5°,
 185 which is around an order of magnitude coarser than the native resolution of state-of-the-art
 186 meteorology reanalysis. Thus, the transport error is expected to significantly affect the flux
 187 estimation in the global inversions. As indicated in the OSSEs, the northern ocean is one of the
 188 regions that can be strongly affected by the transport bias. We further investigate it using real
 189 data assimilation results. A priori of process understanding and oceanic pCO₂ observations in the

190 northern ocean provide a tight constraint on seasonal phase and amplitude of flux (Figure 4a).
 191 However, the a posteriori estimates from the 6 OCO2MIP inversion systems in the northern
 192 ocean diverge greatly during the non-growing seasons of the land biosphere, and the sink during
 193 these seasons is significantly reduced (Figure 4b). It is worth noting that the seasonal phase of
 194 the a posteriori in the CSU system and EXP-real is almost reversed from the a priori estimates.
 195 These seasonal increments from the a priori to the a posteriori are remarkably consistent in phase
 196 and magnitude with the ATM-induced flux bias in EXP-biased, indicating that the ATM bias
 197 highly influences current inversion estimates of ocean carbon fluxes. The temporal correlation
 198 between the flux bias in EXP-biased and the flux increment in EXP-real and CSU is 0.82 and
 199 0.87, respectively. The increments in some inversion systems may not be as significant as in
 200 EXP-real and CSU, which may be because of the different degrees of constraints from the a
 201 priori.



202

203 **Figure 4. (a) The seasonal cycle in the northern extratropical ocean. The blue line is the a**
 204 **posteriori flux in EXP-biased. The orange line is the a posteriori flux in EXP-real. The**
 205 **dark pink line is the a posteriori flux of the ensemble mean of OCO2MIP systems. The thin**
 206 **pink lines with different markers are the individual a posteriori fluxes within the**
 207 **OCO2MIP systems. The black line is the ensemble mean of the a priori fluxes used in the**
 208 **different OCO2MIP systems. The thin gray lines are the individual a priori fluxes used in**
 209 **the OCO2MIP systems. (b) The difference compared with the ensemble mean of the a**
 210 **priori fluxes.**

211 4 Discussion and conclusion

212 Robust regional carbon fluxes estimate is urgently needed within the framework of the United
 213 Nations Framework Convention on Climate Change and is possible as more ground greenhouse
 214 gas stations and satellites are available in the future (Kuhlmann et al., 2020). However, in the
 215 context of OSSEs, this study suggests that the coarse ATM attributes significantly more carbon
 216 uptake in the land and extratropics than in the ocean and tropics. And the seasonal amplitude in
 217 the northern land area is underestimated, which is consistent with a recent finding using aircraft

218 observations (Cui et al., 2022). These robust pieces of evidence indicate that previous inversion
219 studies may largely overestimate the carbon sinks in northern extratropical countries.

220 Focusing on the northern extratropical ocean, we find that the seasonal phase of the a posteriori
221 fluxes totally reverses from the a priori fluxes, compensating for the reduced seasonal amplitude
222 in the northern land area. The reversed phase is also shown in a real data assimilation experiment
223 and some state-of-the-art inversion systems within the OCO2MIP, which is impossible from a
224 process understanding perspective. Satellite observations over the ocean have long been argued
225 to be biased due to retrieval algorithm bias, and inversion modelers usually discard these
226 observations and set tight a priori ocean flux constraints (Peylin et al., 2013; Crowell et al., 2019;
227 Palmer et al., 2019; Peiro et al., 2022). Our finding indicates that the current satellite retrieval
228 algorithm may not be as biased as previously argued, and increasing the resolution of ATM or
229 improving the parameterization schemes of ATM should be placed at a high priority in order to
230 derive a robust country-level carbon budget and reasonable ocean carbon cycle estimates. Recent
231 efforts of speeding up ATMs using Graphics Processing Units (GPU) (Chevallier et al., 2023)
232 and Message Passing Interface (MPI) (Martin et al., 2022) Parallelization are ongoing that native
233 resolution inversion is computationally possible in the coming years.

234 **Acknowledgments**

235 We are grateful to the OCO-2 Flux MIP colleagues for their valuable feedback. We thank
236 Andrew Schuh for the suggestions and comments. This work was supported by the National
237 Natural Science Foundation of China (No. 41975050), the project of “Monitoring, inversion and
238 inventory joint assessment of carbon emissions in typical industrial parks under dual-carbon
239 background” (2022ZJYF001), and the National Key R&D Program of China (grant no.
240 2017YFB0504000).

241 **Conflict of Interest**

242 The authors declare no competing interests.

243 **Data Availability Statement**

244 The OSSE results can be accessed at <https://doi.org/10.5281/zenodo.7826041>. The OCO2MIP
245 inversion results can be accessed from: https://gml.noaa.gov/ccgg/OCO2_v10mip/download.php.
246 The codes related to the COLA can be accessed at <https://doi.org/10.5281/zenodo.7592827> and
247 <https://doi.org/10.5281/zenodo.5746140>.

248 **References**

- 249 Baker, D. F., Bell, E., Davis, K. J., Campbell, J. F., Lin, B., & Dobler, J. (2022). A new
250 exponentially decaying error correlation model for assimilating OCO-2 column-average CO₂
251 data using a length scale computed from airborne lidar measurements. *Geoscientific Model*
252 *Development*, 15(2), 649–668. <https://doi.org/10.5194/gmd-15-649-2022>
253 Basu, S., Baker, D. F., Chevallier, F., Patra, P. K., Liu, J., & Miller, J. B. (2018). The impact of
254 transport model differences on CO₂ surface flux estimates from OCO-2 retrievals of column

- 255 average CO₂. *Atmospheric Chemistry and Physics*, 18(10), 7189–7215.
256 <https://doi.org/10.5194/acp-18-7189-2018>
- 257 Byrne, B., Baker, D. F., Basu, S., Bertolacci, M., Bowman, K. W., Carroll, D., Chatterjee, A.,
258 Chevallier, F., Ciais, P., Cressie, N., Crisp, D., Crowell, S., Deng, F., Deng, Z., Deutscher, N.
259 M., Dubey, M. K., Feng, S., García, O. E., Griffith, D. W. T., ... Zeng, N. (2023). National
260 CO₂ budgets (2015–2020) inferred from atmospheric CO₂ observations in support of the
261 global stocktake. *Earth System Science Data*, 15(2), 963–1004. <https://doi.org/10.5194/essd-15-963-2023>
- 262
263 Chevallier, F. (2021). Fluxes of Carbon Dioxide From Managed Ecosystems Estimated by
264 National Inventories Compared to Atmospheric Inverse Modeling. *Geophysical Research
265 Letters*, 48(15). <https://doi.org/10.1029/2021GL093565>
- 266 Chevallier, F., Lloret, Z., Cozic, A., Takache, S., & Remaud, M. (2023). Toward High-
267 Resolution Global Atmospheric Inverse Modeling Using Graphics Accelerators. *Geophysical
268 Research Letters*, 50(5), e2022GL102135. <https://doi.org/10.1029/2022GL102135>
- 269 Crowell, S., Baker, D., Schuh, A., Basu, S., Jacobson, A. R., Chevallier, F., Liu, J., Deng, F.,
270 Feng, L., McKain, K., Chatterjee, A., Miller, J. B., Stephens, B. B., Eldering, A., Crisp, D.,
271 Schimel, D., Nassar, R., O'Dell, C. W., Oda, T., ... Jones, D. B. A. (2019). The 2015–2016
272 carbon cycle as seen from OCO-2 and the global in situ network. *Atmospheric Chemistry and
273 Physics*, 19(15), 9797–9831. <https://doi.org/10.5194/acp-19-9797-2019>
- 274 Cui, Y. Y., Zhang, L., Jacobson, A. R., Johnson, M. S., Philip, S., Baker, D., Chevallier, F.,
275 Schuh, A. E., Liu, J., Crowell, S., Peiro, H. E., Deng, F., Basu, S., & Davis, K. J. (2022).
276 Evaluating Global Atmospheric Inversions of Terrestrial Net Ecosystem Exchange CO₂ Over
277 North America on Seasonal and Sub-Continental Scales. *Geophysical Research Letters*,
278 49(18). <https://doi.org/10.1029/2022GL100147>
- 279 Deng, Z., Ciais, P., Tzompa-Sosa, Z. A., Saunio, M., Qiu, C., Tan, C., Sun, T., Ke, P., Cui, Y.,
280 Tanaka, K., Lin, X., Thompson, R. L., Tian, H., Yao, Y., Huang, Y., Lauerwald, R., Jain, A.
281 K., Xu, X., Bastos, A., ... Chevallier, F. (2022). Comparing national greenhouse gas budgets
282 reported in UNFCCC inventories against atmospheric inversions. *Earth System Science Data*,
283 14(4), 1639–1675. <https://doi.org/10.5194/essd-14-1639-2022>
- 284 Friedlingstein, P., Jones, M. W., O'Sullivan, M., Andrew, R. M., Bakker, D. C. E., Hauck, J., Le
285 Quéré, C., Peters, G. P., Peters, W., Pongratz, J., Sitch, S., Canadell, J. G., Ciais, P., Jackson,
286 R. B., Alin, S. R., Anthoni, P., Bates, N. R., Becker, M., Bellouin, N., ... Zeng, J. (2022).
287 Global Carbon Budget 2021. *Earth System Science Data*, 14(4), 1917–2005.
288 <https://doi.org/10.5194/essd-14-1917-2022>
- 289 Fu, Y., Liao, H., Tian, X., Gao, H., Jia, B., & Han, R. (2021). Impact of Prior Terrestrial Carbon
290 Fluxes on Simulations of Atmospheric CO₂ Concentrations. *Journal of Geophysical
291 Research: Atmospheres*, 126(18). <https://doi.org/10.1029/2021JD034794>
- 292 Gelaro, R., McCarty, W., Suárez, M. J., Todling, R., Molod, A., Takacs, L., Randles, C. A.,
293 Darmenov, A., Bosilovich, M. G., Reichle, R., Wargan, K., Coy, L., Cullather, R., Draper, C.,
294 Akella, S., Buchard, V., Conaty, A., da Silva, A. M., Gu, W., ... Zhao, B. (2017). The
295 Modern-Era Retrospective Analysis for Research and Applications, Version 2 (MERRA-2).
296 *Journal of Climate*, 30(14), 5419–5454. <https://doi.org/10.1175/JCLI-D-16-0758.1>
- 297 Haynes, K. D., Baker, I. T., Denning, A. S., Stöckli, R., Schaefer, K., Lokupitiya, E. Y., &
298 Haynes, J. M. (2019). Representing Grasslands Using Dynamic Prognostic Phenology Based
299 on Biological Growth Stages: 1. Implementation in the Simple Biosphere Model (SiB4).

- 300 *Journal of Advances in Modeling Earth Systems*, 11(12), 4423–4439.
301 <https://doi.org/10.1029/2018MS001540>
- 302 Jiang, F., He, W., Ju, W., Wang, H., Wu, M., Wang, J., Feng, S., Zhang, L., & Chen, J. M.
303 (2022). The status of carbon neutrality of the world's top 5 CO₂ emitters as seen by carbon
304 satellites. *Fundamental Research*, 2(3), 357–366. <https://doi.org/10.1016/j.fmre.2022.02.001>
- 305 Kaiser, J. W., Heil, A., Andreae, M. O., Benedetti, A., Chubarova, N., Jones, L., Morcrette, J.-J.,
306 Razinger, M., Schultz, M. G., Suttie, M., & van der Werf, G. R. (2012). Biomass burning
307 emissions estimated with a global fire assimilation system based on observed fire radiative
308 power. *Biogeosciences*, 9(1), 527–554. <https://doi.org/10.5194/bg-9-527-2012>
- 309 Kuhlmann, G., Brunner, D., Broquet, G., & Meijer, Y. (2020). Quantifying CO₂ emissions of a
310 city with the Copernicus Anthropogenic CO₂ Monitoring satellite mission. *Atmospheric
311 Measurement Techniques*, 13(12), 6733–6754. <https://doi.org/10.5194/amt-13-6733-2020>
- 312 Liu, J., Fung, I., Kalnay, E., & Kang, J.-S. (2011). CO₂ transport uncertainties from the
313 uncertainties in meteorological fields. *Geophysical Research Letters*, 38, L12808.
314 <https://doi.org/10.1029/2011GL047213>
- 315 Liu, Z., Zeng, N., Liu, Y., Kalnay, E., Asrar, G., Cai, Q., & Han, P. (2023). *Assimilating the
316 dynamic spatial gradient of a bottom-up carbon flux estimation as a unique observation in
317 COLA (v2.0)*. <https://doi.org/10.5194/gmd-2023-15>
- 318 Liu, Z., Zeng, N., Liu, Y., Kalnay, E., Asrar, G., Wu, B., Cai, Q., Liu, D., & Han, P. (2022).
319 Improving the joint estimation of CO₂ and surface carbon fluxes using a constrained ensemble
320 Kalman filter in COLA (v1.0). *Geosci. Model Dev.*, 15, 5511–5528.
321 <https://doi.org/10.5194/gmd-15-5511-2022>
- 322 Martin, R. V., Eastham, S. D., Bindle, L., Lundgren, E. W., Clune, T. L., Keller, C. A., Downs,
323 W., Zhang, D., Lucchesi, R. A., Sulprizio, M. P., Yantosca, R. M., Li, Y., Estrada, L., Putman,
324 W. M., Auer, B. M., Trayanov, A. L., Pawson, S., & Jacob, D. J. (2022). Improved advection,
325 resolution, performance, and community access in the new generation (version 13) of the
326 high-performance GEOS-Chem global atmospheric chemistry model (GCHP). *Geoscientific
327 Model Development*, 15(23), 8731–8748. <https://doi.org/10.5194/gmd-15-8731-2022>
- 328 Oda, T., Maksyutov, S., & Andres, R. J. (2018). The Open-source Data Inventory for
329 Anthropogenic CO₂, version 2016 (ODIAC2016): A global monthly fossil fuel CO₂ gridded
330 emissions data product for tracer transport simulations and surface flux inversions. *Earth
331 System Science Data*, 10(1), 87–107. <https://doi.org/10.5194/essd-10-87-2018>
- 332 O'Dell, C. W., Eldering, A., Wennberg, P. O., Crisp, D., Gunson, M. R., Fisher, B.,
333 Frankenberg, C., Kiel, M., Lindqvist, H., Mandrake, L., Merrelli, A., Natraj, V., Nelson, R. R.,
334 Osterman, G. B., Payne, V. H., Taylor, T. E., Wunch, D., Drouin, B. J., Oyafuso, F., ...
335 Velasco, V. A. (2018). Improved retrievals of carbon dioxide from Orbiting Carbon
336 Observatory-2 with the version 8 ACOS algorithm. *Atmospheric Measurement Techniques*,
337 11(12), 6539–6576. <https://doi.org/10.5194/amt-11-6539-2018>
- 338 Palmer, P. I., Feng, L., Baker, D., Chevallier, F., Bösch, H., & Somkuti, P. (2019). Net carbon
339 emissions from African biosphere dominate pan-tropical atmospheric CO₂ signal. *Nature
340 Communications*, 10(1), 3344. <https://doi.org/10.1038/s41467-019-11097-w>
- 341 Peiro, H., Crowell, S., Schuh, A., Baker, D. F., O'Dell, C., Jacobson, A. R., Chevallier, F., Liu,
342 J., Eldering, A., Crisp, D., Deng, F., Weir, B., Basu, S., Johnson, M. S., Philip, S., & Baker, I.
343 (2022). Four years of global carbon cycle observed from the Orbiting Carbon Observatory 2
344 (OCO-2) version 9 and in situ data and comparison to OCO-2 version 7. *Atmospheric
345 Chemistry and Physics*, 22(2), 1097–1130. <https://doi.org/10.5194/acp-22-1097-2022>

- 346 Peylin, P., Law, R. M., Gurney, K. R., Chevallier, F., Jacobson, A. R., Maki, T., Niwa, Y., Patra,
347 P. K., Peters, W., Rayner, P. J., Rödenbeck, C., van der Laan-Luijkx, I. T., & Zhang, X.
348 (2013). Global atmospheric carbon budget: Results from an ensemble of atmospheric
349 CO₂ inversions. *Biogeosciences*, *10*(10), 6699–6720.
350 <https://doi.org/10.5194/bg-10-6699-2013>
- 351 Philip, S., Johnson, M. S., Potter, C., Genovesse, V., Baker, D. F., Haynes, K. D., Henze, D. K.,
352 Liu, J., & Poulter, B. (2019). Prior biosphere model impact on global terrestrial CO₂ fluxes
353 estimated from OCO-2 retrievals. *Atmospheric Chemistry and Physics*, *19*(20), 13267–13287.
354 <https://doi.org/10.5194/acp-19-13267-2019>
- 355 Rödenbeck, C., Bakker, D. C. E., Metzl, N., Olsen, A., Sabine, C., Cassar, N., Reum, F.,
356 Keeling, R. F., & Heimann, M. (2014). Interannual sea–air CO₂ flux variability from an
357 observation-driven ocean mixed-layer scheme. *Biogeosciences*, *11*(17), 4599–4613.
358 <https://doi.org/10.5194/bg-11-4599-2014>
- 359 Schimel, D., Stephens, B. B., & Fisher, J. B. (2015). Effect of increasing CO₂ on the terrestrial
360 carbon cycle. *Proceedings of the National Academy of Sciences*, *112*(2), 436–441.
361 <https://doi.org/10.1073/pnas.1407302112>
- 362 Schuh, A. E., Byrne, B., Jacobson, A. R., Crowell, S. M. R., Deng, F., Baker, D. F., Johnson, M.
363 S., Philip, S., & Weir, B. (2022). On the role of atmospheric model transport uncertainty in
364 estimating the Chinese land carbon sink. *Nature*, *603*(7901), E13–E14.
365 <https://doi.org/10.1038/s41586-021-04258-9>
- 366 Schuh, A. E., & Jacobson, A. R. (2022). Uncertainty in Parameterized Convection Remains a
367 Key Obstacle for Estimating Surface Fluxes of Carbon Dioxide. *Atmospheric Chemistry and*
368 *Physics Discussion [Preprint]*. <https://doi.org/10.5194/acp-2022-616>
- 369 Schuh, A. E., Jacobson, A. R., Basu, S., Weir, B., Baker, D., Bowman, K., Chevallier, F.,
370 Crowell, S., Davis, K. J., Deng, F., Denning, S., Feng, L., Jones, D., Liu, J., & Palmer, P. I.
371 (2019). Quantifying the Impact of Atmospheric Transport Uncertainty on CO₂ Surface Flux
372 Estimates. *Global Biogeochemical Cycles*, *33*(4), 484–500.
373 <https://doi.org/10.1029/2018GB006086>
- 374 Stephens, B. B., Gurney, K. R., Tans, P. P., Sweeney, C., Peters, W., Bruhwiler, L., Ciais, P.,
375 Ramonet, M., Bousquet, P., Nakazawa, T., Aoki, S., Machida, T., Inoue, G., Vinnichenko, N.,
376 Lloyd, J., Jordan, A., Heimann, M., Shibistova, O., Langenfelds, R. L., ... Denning, A. S.
377 (2007). Weak Northern and Strong Tropical Land Carbon Uptake from Vertical Profiles of
378 Atmospheric CO₂. *Science*, *316*(5832), 1732–1735. <https://doi.org/10.1126/science.1137004>
- 379 The International GEOS-Chem User Community. (2021). *geoschem/GCClassic: GEOS-Chem*
380 *13.0.2* (13.0.2). Zenodo. <https://doi.org/10.5281/ZENODO.4681204>
- 381 Wang, J., Feng, L., Palmer, P. I., Liu, Y., Fang, S., Bösch, H., O'Dell, C. W., Tang, X., Yang,
382 D., Liu, L., & Xia, C. (2020). Large Chinese land carbon sink estimated from atmospheric
383 carbon dioxide data. *Nature*, *586*(7831), 720–723. <https://doi.org/10.1038/s41586-020-2849-9>
- 384 Weir, B., Oda, T., Ott, L. E., & Schmidt, G. A. (2022). Assessing progress toward the Paris
385 Climate Agreement from Space. *Environmental Research Letters*.
386 <https://doi.org/10.1088/1748-9326/ac998c>
- 387 Yu, K., Keller, C. A., Jacob, D. J., Molod, A. M., Eastham, S. D., & Long, M. S. (2018). Errors
388 and improvements in the use of archived meteorological data for chemical transport modeling:
389 An analysis using GEOS-Chem v11-01 driven by GEOS-5 meteorology. *Geoscientific Model*
390 *Development*, *11*(1), 305–319. <https://doi.org/10.5194/gmd-11-305-2018>

1 **Large impact of coarse-resolution atmospheric transport model error on land-ocean**
2 **and tropic-extratropic partitioning and seasonal cycle in CO₂ inversion**
3

4 **Zhiqiang Liu^{1,2}, Ning Zeng^{3,4}, Pengfei Han^{5,1}, Qixiang Cai¹**

5 ¹Laboratory of Numerical Modeling for Atmospheric Sciences & Geophysical Fluid Dynamics,
6 Institute of Atmospheric Physics, Chinese Academy of Sciences, Beijing, China

7 ²University of Chinese Academy of Sciences, Beijing, China

8 ³Dept. of Atmospheric and Oceanic Science, University of Maryland, USA

9 ⁴Earth System Science Interdisciplinary Center, University of Maryland, USA

10 ⁵Carbon Neutrality Research Center, Institute of Atmospheric Physics, Chinese Academy of
11 Sciences, Beijing, China

12 Corresponding authors: Zhiqiang Liu (liuzhiqiang@mail.iap.ac.cn)

13 **Key Points:**

- 14 ● Error from the coarse-resolution atmospheric transport model can introduce systematic
15 biases to CO₂ modeling and inversed flux estimates.
- 16 ● The coarse-resolution transport error leads to stronger land and extratropical sink
17 estimates and weaker ocean and tropical sink estimates.
- 18 ● The error also induces an underestimated seasonal amplitude and a reversed seasonal
19 phase in the northern land and ocean, respectively.

20 **Abstract**

21 We show that forward simulations of global CO₂ using an atmospheric transport model (ATM) at
22 0.5° × 0.625° and 4° × 5° resolutions differ significantly in vertical and meridional distribution.
23 Comparing two observing simulation system experiments at 4° × 5° resolution that assimilate
24 pseudo observations sampled from the two forward simulations, we isolated the impact of
25 coarse-resolution ATM error on regional flux estimates that a significant amount of annual
26 carbon uptake from the ocean and tropics is improperly redistributed to the land and extratropics,
27 respectively. In addition, this error leads to an underestimated seasonal amplitude in the northern
28 extratropical land and a reversed seasonal phase in the northern extratropical ocean. The reversed
29 seasonal phase has also been shown in a real data assimilation experiment and state-of-the-art
30 inversions, suggesting that ocean glint retrieval error may not be as significant as previously
31 thought and reasonable ocean flux estimates depend strongly on the accuracy of ATM.

32 **Plain Language Summary**

33 Credible regional carbon budget estimates from atmospheric CO₂ measurements rely on the
34 accuracy of atmospheric transport models (ATMs). However, the simulated atmospheric vertical
35 motions in ATMs are usually simplified and spatiotemporally averaged, leading to systematic
36 biases in simulating the long-lived atmospheric CO₂ and estimating surface carbon fluxes. Even
37 though the atmospheric approach is increasingly applied to account for country-level carbon
38 budget in global synthesis activities. Our finding suggests that current coarse-resolution ATMs
39 lead to improper attribution of annual carbon uptake from the ocean and tropics to the land and
40 extratropics, respectively, resulting in overestimated natural carbon uptake and reduced
41 emissions reduction duty in most advanced countries that target carbon neutrality. Furthermore,
42 since the seasonal variation of carbon flux in the ocean is much smaller than in the land, the
43 results indicate that a small seasonal bias from the land can overwrite and even reverse the real
44 flux signal in the ocean.

45 **1 Introduction**

46 Quantifying the country-level CO₂ budget using atmospheric CO₂ inversion technique is
47 one of the critical approaches in the upcoming Global StockTake assessment (Chevallier, 2021;
48 Jiang et al., 2022; Weir et al., 2022; Deng et al., 2022; Byrne et al., 2023). However, several
49 fundamental issues in CO₂ inversion (e.g., transport, satellite retrieval, and a priori errors) have
50 not been fully addressed, challenging the derivation of robust regional CO₂ budget estimation
51 (Fu et al., 2021; O'Dell et al., 2018; Philip et al., 2019; Schuh et al., 2019). Inversion systems
52 use an offline atmosphere transport model (ATM) to relate the surface land and ocean carbon
53 fluxes with observed CO₂ concentration. An offline ATM is driven by the meteorology
54 reanalysis data generated from a general circulation model (GCM), which significantly reduces
55 the computational cost but simplifies and spatiotemporally averages some nonlinear atmospheric
56 processes (J. Liu et al., 2011; Basu et al., 2018; Schuh et al., 2019). The averaging processes
57 include remapping the GCM output from seconds to hours and irregular grid to latitude-
58 longitude grid, and spatial interpolation from native to coarse horizontal resolution, which
59 induces underestimated transient vertical motion and reduced vertical transport (Yu et al., 2018).
60 Recent forward modeling studies find that the simulated CO₂ concentrations are significantly
61 different in vertical and meridional distribution using different ATM configurations and ATMs
62 (Schuh et al., 2019; Schuh & Jacobson, 2022). These biases can influence the estimates of

63 regional carbon budgets (Wang et al., 2020; Schuh et al., 2022) and seasonal cycles (Cui et al.,
64 2022) estimates. A large discrepancy between the inversion estimates and process
65 understandings is the land-ocean and tropic-extratropic partitioning of carbon fluxes. The
66 inversions usually estimate a large carbon sink in the northern extratropics and a weak carbon
67 sink or carbon source in the tropics recently, while process models or inventories suggest more
68 carbon uptake in the tropics (Schimel et al., 2015; Friedlingstein et al., 2022). Evidence from the
69 vertical CO₂ observation profiles indicates that inversions may overestimate the northern sink
70 and underestimate the tropical sink (Stephens et al., 2007).

71 To reduce the main transport error, running global inversions at the native resolution is a
72 straightforward strategy. However, native resolution inversions can be very slow due to reading
73 and writing a large amount of data and poor parallel methods in some ATMs (e.g., classic
74 GEOS-Chem) (The International GEOS-Chem User Community, 2021). For example, forward
75 simulation of global CO₂ at a native horizontal resolution of $0.5^\circ \times 0.625^\circ$ using GEOS-Chem
76 requires around 60 gigabytes (GB) of memory and could be paralleled using OpenMP only that a
77 one-year simulation costs more than 1 week using 1 Central Processing Unit (CPU) with 20
78 cores. The computation costs will increase dramatically by at least an order of magnitude when
79 conducting ensemble or adjoint simulation, thus not possible in real inversion applications but
80 acceptable in simple forward simulation. In this study, instead of conducting native inversion
81 directly, we, for the first time, derived the impact of coarse resolution transport model error on
82 large-scale flux distribution in the context of observing simulation system experiments (OSSEs)
83 and further suggested that the estimated northern ocean fluxes in current state-of-the-art
84 inversion systems are likely driven by the transport error instead of observation information or
85 satellite retrieval errors. Section 2 describes the data and method; Section 3 shows the results; the
86 conclusion and discussion are presented in the last section.

87 **2 Data and method**

88 We use the Carbon in Ocean-Land-Atmosphere (COLA) system (Z. Liu et al., 2022,
89 2023) to understand the transport impact on flux estimation in the context of Observing
90 Simulation System Experiments (OSSEs) and a real data assimilation experiment. COLA
91 optimizes the land (F_{TA}) and ocean (F_{OA}) carbon fluxes using a local ensemble transform Kalman
92 filter and a constrained ensemble Kalman filter, while terrestrial fire flux (F_{IR}) and anthropogenic
93 fossil fuel emissions (F_{FE}) are not optimized. The atmosphere transport model used in COLA is
94 GEOS-Chem of version 13.0.2, driven by the Modern-Era Retrospective analysis for Research
95 and Applications Version 2 (MERRA-2) meteorology reanalysis (Gelaro et al., 2017; The
96 International GEOS-Chem User Community, 2021). The native spatial resolution of MERRA-2
97 is $0.5^\circ \times 0.625^\circ$.

98 In this study, two sets of OSSEs are performed from December 2014 to the end of 2015.
99 In the first OSSE (EXP-biased), the assimilation run is conducted at $4^\circ \times 5^\circ$ resolution while the
100 nature run is conducted at the native $0.5^\circ \times 0.625^\circ$ resolution. In the second OSSE (EXP-perfect),
101 both the assimilation run and nature run are conducted at $4^\circ \times 5^\circ$ resolution. The pseudo surface
102 and satellite observation network are almost identical to Liu et al. (2022) but with additional
103 ocean glint observations from the Orbiting Carbon Observatory-2 (OCO-2) (O'Dell et al., 2018;
104 Baker et al., 2022). This kind of observation network was usually called LNLGOGIS in the
105 OCO-2 flux model intercomparison project (OCO2MIP) (Crowell et al., 2019; Peiro et al., 2022;
106 Byrne et al., 2023). Then the pseudo observations in each OSSE are sampled from their

107 corresponding nature runs and randomly perturbed based on the error scales described in Liu et
108 al. (2022). The nature runs start from the same initial CO₂ concentration and are forced by
109 identical surface carbon fluxes with the F_{FE} from the Open-source Data Inventory of
110 Anthropogenic CO₂ emissions (ODIAC) (Oda et al., 2018), the F_{IR} from Global Fire
111 Assimilation System (GFAS) (Kaiser et al., 2012), the F_{OA} from Rödenbeck et al. (2014), and the
112 F_{TA} generated from the terrestrial model of Simple Biosphere Model Version 4 (SiB4) (Haynes
113 et al., 2019). To separate the impact of model resolution while with less impact from a priori
114 fluxes, the a priori F_{TA} and F_{OA} used in the assimilation runs are similar as in the nature runs but
115 from 4 years ago.

116 In addition to the two OSSEs, a real data assimilation experiment (EXP-real) is
117 conducted at 4° × 5° resolution that assimilates the LNLGOGIS observations. And the a priori
118 fluxes and assimilation period are identical to the nature run of EXP-biased. An ensemble of
119 global inversion results (Ames, Baker, CSU, CT, OU, and TM5-4DVAR) within version 10 of
120 OCO2MIP that assimilate the LNLGOGIS observations and without very tight ocean a priori
121 constraint is used to validate the transport bias impact further (Byrne et al., 2023). Moreover, 4 a
122 priori of "bottom-up" ocean flux products in the OCO2MIP systems are used as references.

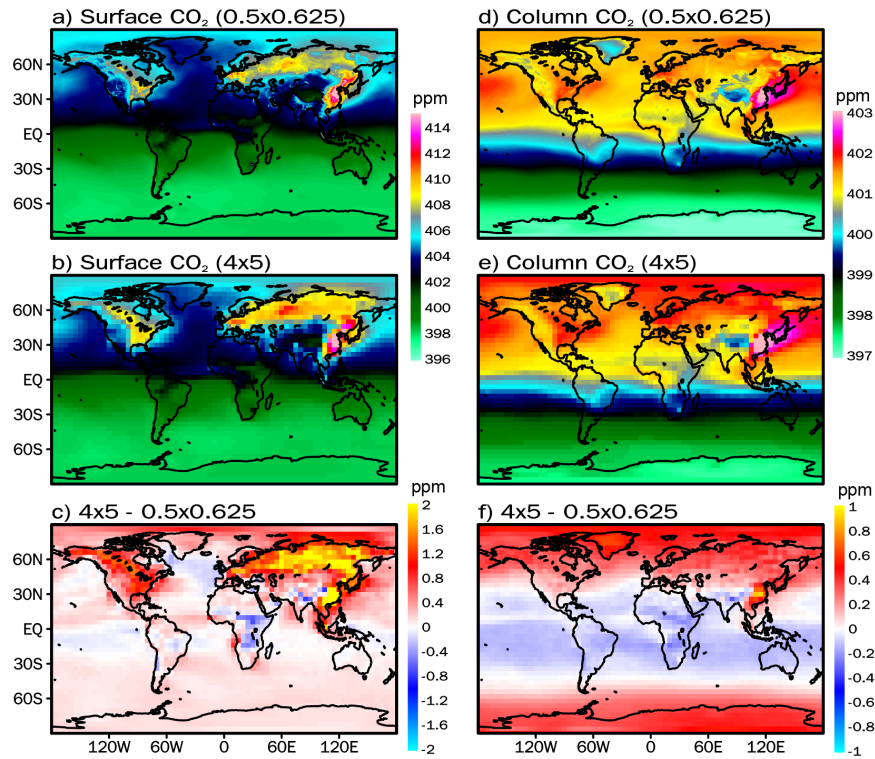
123 **3 Results**

124 **3.1 Land-ocean and tropic-extratropic partitioning**

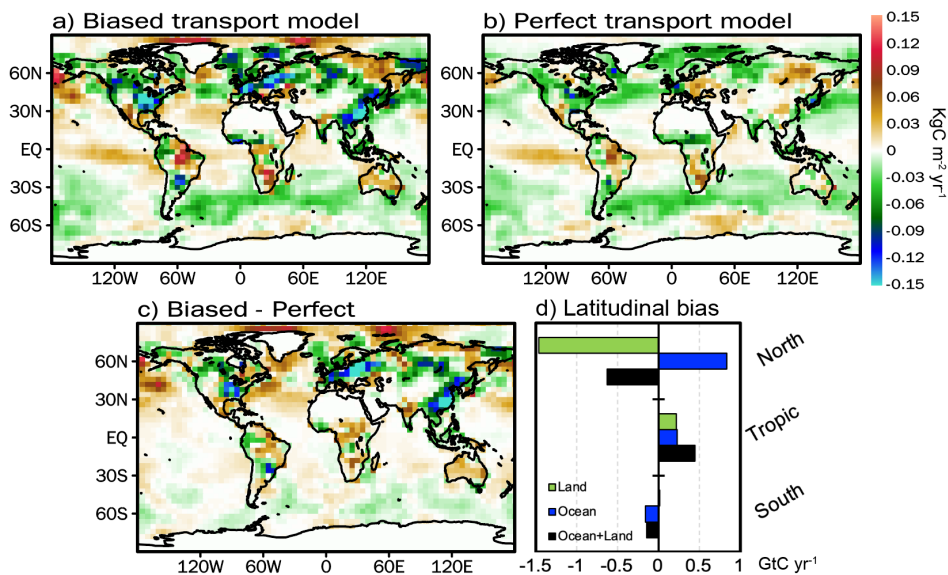
125 First, we analyze the surface CO₂ and column CO₂ (XCO₂) concentration in the nature
126 runs of EXP-bias (Figure 1a, d) and EXP-perfect (Figure 1b, e). Even though the two nature runs
127 are driven by the same surface fluxes (Figure S1), the biased ATM at 4° × 5° resolution tends to
128 trap the CO₂ fluxes within the near-surface in the Northern Hemisphere than the ATM at native
129 0.5° × 0.625° resolution on an annual average basis, especially in Eurasia that the biases can
130 reach to over 2 ppm. The XCO₂ bias has clear latitudinal distribution with positive bias in the
131 Northern (30°N~ 90°N) and Southern (-90°S~ -30°S) middle and high latitudes and negative
132 bias near the tropics (-30°S~ 30°N). Moreover, the annual bias is averaged from the seasonal
133 varying biases. In Eurasia, the positive surface bias of over 5 ppm from January to March is
134 reversed to the negative surface bias of over -3 ppm from July to September (Figure S2, S3). The
135 seasonal variation of XCO₂ bias is relatively smaller than the surface CO₂. The persistent dipole
136 tropic versus extratropic bias pattern moves southward from winter to summer.

137 The systematic error of simulated CO₂ concentration caused by the coarse-resolution
138 ATM is expected to cause significant bias in flux estimates. The first assimilation run of EXP-
139 biased assimilates the "perfect" observations but uses the "biased" ATM, which is similar to the
140 real-world scenario. Instead, the second assimilation run of EXP-perfect has no transport model
141 error issue that assimilates the "perfect" observations and uses the "perfect" ATM. The
142 difference in estimated fluxes between the two assimilation runs is expected to be the impact of
143 transport error on flux estimation. Annually, the absolute value of regional land fluxes in EXP-
144 biased is significantly larger than EXP-perfect (Figure 2a, b). In the northern mid-latitudes land
145 area, the carbon sink is largely overestimated in EXP-biased, especially in eastern China, eastern
146 North America, and Europe. About half of this sink is compensated by the surrounding
147 weakened ocean sink and carbon release in the high latitude of East Siberia (Figure 2d). Moving
148 southward, EXP-biased shows less carbon sink in the tropical ocean, South America, Australia,
149 and Africa and more carbon sink in the Southern Ocean. Generally, relative to EXP-perfect, the

150 transport error tends to enhance the land carbon sink by 1.23 GtC yr⁻¹ and weaken the ocean
 151 carbon sink by 0.9 GtC yr⁻¹. Moreover, more carbon sink of 0.77 GtC yr⁻¹ is attributed to the
 152 extratropics (-90 °S~ -23 °S and 23 °N~ 90 °N), and 0.44 GtC yr⁻¹ more carbon is released from
 153 the tropics (-23 °S~ 23 °N), resulting in a global net flux bias of -0.33 GtC yr⁻¹. Due to the high
 154 computation and memory cost, we only conduct tests for 1 year. Further research on how ATM
 155 bias affects interannual flux estimation is worth investigating in the future.



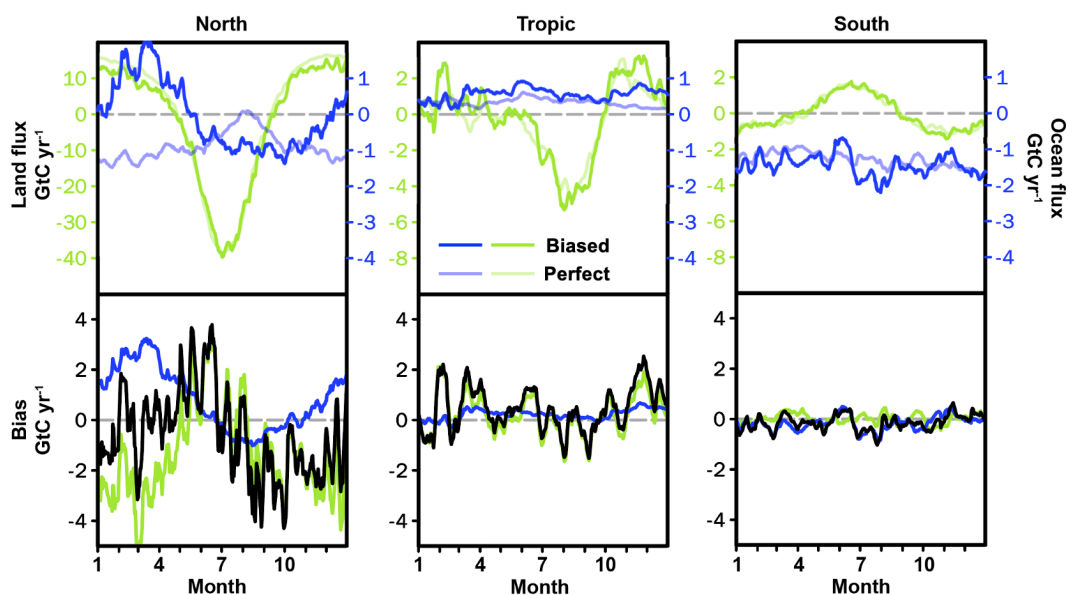
156 **Figure 1. The annual mean surface CO₂ and column CO₂ pattern of nature runs at**
 157 **horizontal resolutions of 0.5° × 0.625° (a, d) and 4° × 5° (b, e). (c, f) The difference between**
 158 **the two nature runs.**
 159



161 **Figure 2. The spatial pattern of optimized annual mean land and ocean fluxes of**
 162 **assimilation runs of EXP-biased (a) and EXP-perfect (b). (c) The difference between the**
 163 **two assimilation runs. (d) The difference in land and ocean fluxes between the two**
 164 **assimilation runs in latitude bands of northern extratropics (23 °N ~ 90 °N), tropics (-23 °S**
 165 **~ 23 °N), and southern extratropics (-90 °S ~ -23 °S).**

166 3.2 Seasonal cycle

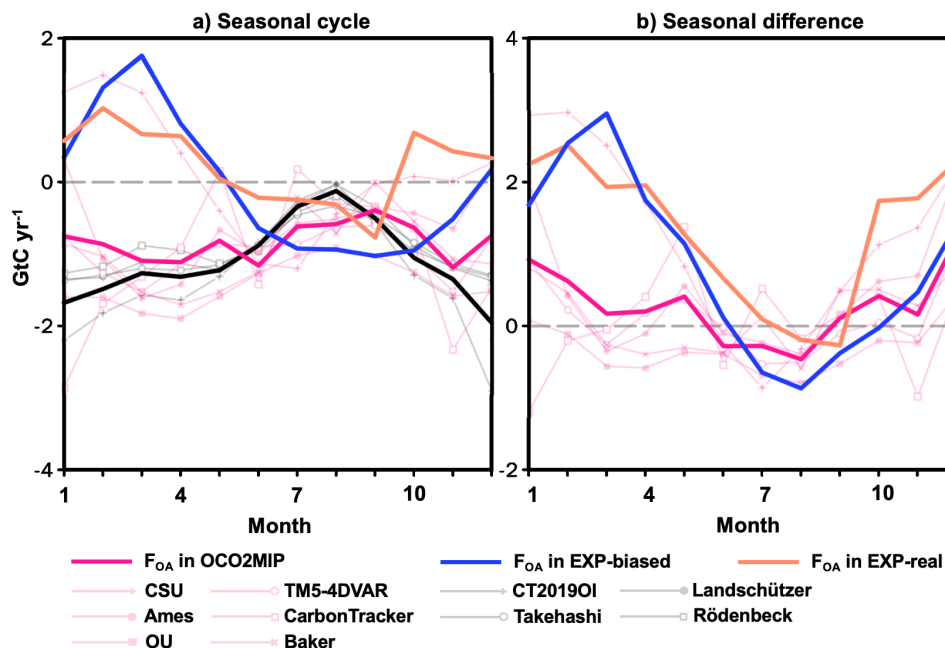
167 At the seasonal scale, the seasonal amplitude of the northern extratropical land flux is
 168 significantly underestimated in EXP-biased, mainly due to less carbon release during the non-
 169 growing seasons (Figure 3). In the northern extratropical ocean, the seasonal phase is reversed
 170 and the seasonal strength is enhanced, which partly compensates for the weakened seasonal
 171 amplitude in the northern extratropical land. The seasonal biases are smaller in the tropics and
 172 southern extratropics. From January to May, a large amount of carbon is released from the
 173 northern ocean. And the relative impact of transport error on the ocean flux is significantly larger
 174 than the land flux, implying that the ocean flux estimation in the context of the transport error
 175 may not be better than those a priori estimations. To overcome this limitation, inverse modelers
 176 usually apply tight a priori constraints on ocean flux in the real-world scenario (Peylin et al.,
 177 2013).



178 **Figure 3. The upper figures are the seasonal cycle of land (green) and ocean (blue) fluxes**
 179 **of EXP-biased (darker color) and EXP-perfect (lighter color) at daily timestep in latitude**
 180 **bands of northern extratropics (23 °N ~ 90 °N), tropics (-23 °S ~ 23 °N), and southern**
 181 **extratropics (-90 °S ~ -23 °S). The bottom figures are the land, ocean, and net (black) fluxes**
 182 **difference between EXP-biased and EXP-perfect.**

184 Global inversion systems were usually run at a coarse horizontal resolution of 2° to 5°,
 185 which is around an order of magnitude coarser than the native resolution of state-of-the-art
 186 meteorology reanalysis. Thus, the transport error is expected to significantly affect the flux
 187 estimation in the global inversions. As indicated in the OSSEs, the northern ocean is one of the
 188 regions that can be strongly affected by the transport bias. We further investigate it using real
 189 data assimilation results. A priori of process understanding and oceanic pCO₂ observations in the

190 northern ocean provide a tight constraint on seasonal phase and amplitude of flux (Figure 4a).
 191 However, the a posteriori estimates from the 6 OCO2MIP inversion systems in the northern
 192 ocean diverge greatly during the non-growing seasons of the land biosphere, and the sink during
 193 these seasons is significantly reduced (Figure 4b). It is worth noting that the seasonal phase of
 194 the a posteriori in the CSU system and EXP-real is almost reversed from the a priori estimates.
 195 These seasonal increments from the a priori to the a posteriori are remarkably consistent in phase
 196 and magnitude with the ATM-induced flux bias in EXP-biased, indicating that the ATM bias
 197 highly influences current inversion estimates of ocean carbon fluxes. The temporal correlation
 198 between the flux bias in EXP-biased and the flux increment in EXP-real and CSU is 0.82 and
 199 0.87, respectively. The increments in some inversion systems may not be as significant as in
 200 EXP-real and CSU, which may be because of the different degrees of constraints from the a
 201 priori.



202

203 **Figure 4. (a) The seasonal cycle in the northern extratropical ocean. The blue line is the a**
 204 **posteriori flux in EXP-biased. The orange line is the a posteriori flux in EXP-real. The**
 205 **dark pink line is the a posteriori flux of the ensemble mean of OCO2MIP systems. The thin**
 206 **pink lines with different markers are the individual a posteriori fluxes within the**
 207 **OCO2MIP systems. The black line is the ensemble mean of the a priori fluxes used in the**
 208 **different OCO2MIP systems. The thin gray lines are the individual a priori fluxes used in**
 209 **the OCO2MIP systems. (b) The difference compared with the ensemble mean of the a**
 210 **priori fluxes.**

211 4 Discussion and conclusion

212 Robust regional carbon fluxes estimate is urgently needed within the framework of the United
 213 Nations Framework Convention on Climate Change and is possible as more ground greenhouse
 214 gas stations and satellites are available in the future (Kuhlmann et al., 2020). However, in the
 215 context of OSSEs, this study suggests that the coarse ATM attributes significantly more carbon
 216 uptake in the land and extratropics than in the ocean and tropics. And the seasonal amplitude in
 217 the northern land area is underestimated, which is consistent with a recent finding using aircraft

218 observations (Cui et al., 2022). These robust pieces of evidence indicate that previous inversion
219 studies may largely overestimate the carbon sinks in northern extratropical countries.

220 Focusing on the northern extratropical ocean, we find that the seasonal phase of the a posteriori
221 fluxes totally reverses from the a priori fluxes, compensating for the reduced seasonal amplitude
222 in the northern land area. The reversed phase is also shown in a real data assimilation experiment
223 and some state-of-the-art inversion systems within the OCO2MIP, which is impossible from a
224 process understanding perspective. Satellite observations over the ocean have long been argued
225 to be biased due to retrieval algorithm bias, and inversion modelers usually discard these
226 observations and set tight a priori ocean flux constraints (Peylin et al., 2013; Crowell et al., 2019;
227 Palmer et al., 2019; Peiro et al., 2022). Our finding indicates that the current satellite retrieval
228 algorithm may not be as biased as previously argued, and increasing the resolution of ATM or
229 improving the parameterization schemes of ATM should be placed at a high priority in order to
230 derive a robust country-level carbon budget and reasonable ocean carbon cycle estimates. Recent
231 efforts of speeding up ATMs using Graphics Processing Units (GPU) (Chevallier et al., 2023)
232 and Message Passing Interface (MPI) (Martin et al., 2022) Parallelization are ongoing that native
233 resolution inversion is computationally possible in the coming years.

234 **Acknowledgments**

235 We are grateful to the OCO-2 Flux MIP colleagues for their valuable feedback. We thank
236 Andrew Schuh for the suggestions and comments. This work was supported by the National
237 Natural Science Foundation of China (No. 41975050), the project of “Monitoring, inversion and
238 inventory joint assessment of carbon emissions in typical industrial parks under dual-carbon
239 background” (2022ZJYF001), and the National Key R&D Program of China (grant no.
240 2017YFB0504000).

241 **Conflict of Interest**

242 The authors declare no competing interests.

243 **Data Availability Statement**

244 The OSSE results can be accessed at <https://doi.org/10.5281/zenodo.7826041>. The OCO2MIP
245 inversion results can be accessed from: https://gml.noaa.gov/ccgg/OCO2_v10mip/download.php.
246 The codes related to the COLA can be accessed at <https://doi.org/10.5281/zenodo.7592827> and
247 <https://doi.org/10.5281/zenodo.5746140>.

248 **References**

- 249 Baker, D. F., Bell, E., Davis, K. J., Campbell, J. F., Lin, B., & Dobler, J. (2022). A new
250 exponentially decaying error correlation model for assimilating OCO-2 column-average CO₂
251 data using a length scale computed from airborne lidar measurements. *Geoscientific Model*
252 *Development*, 15(2), 649–668. <https://doi.org/10.5194/gmd-15-649-2022>
253 Basu, S., Baker, D. F., Chevallier, F., Patra, P. K., Liu, J., & Miller, J. B. (2018). The impact of
254 transport model differences on CO₂ surface flux estimates from OCO-2 retrievals of column

- 255 average CO₂. *Atmospheric Chemistry and Physics*, 18(10), 7189–7215.
256 <https://doi.org/10.5194/acp-18-7189-2018>
- 257 Byrne, B., Baker, D. F., Basu, S., Bertolacci, M., Bowman, K. W., Carroll, D., Chatterjee, A.,
258 Chevallier, F., Ciais, P., Cressie, N., Crisp, D., Crowell, S., Deng, F., Deng, Z., Deutscher, N.
259 M., Dubey, M. K., Feng, S., García, O. E., Griffith, D. W. T., ... Zeng, N. (2023). National
260 CO₂ budgets (2015–2020) inferred from atmospheric CO₂ observations in support of the
261 global stocktake. *Earth System Science Data*, 15(2), 963–1004. <https://doi.org/10.5194/essd-15-963-2023>
- 262
263 Chevallier, F. (2021). Fluxes of Carbon Dioxide From Managed Ecosystems Estimated by
264 National Inventories Compared to Atmospheric Inverse Modeling. *Geophysical Research
265 Letters*, 48(15). <https://doi.org/10.1029/2021GL093565>
- 266 Chevallier, F., Lloret, Z., Cozic, A., Takache, S., & Remaud, M. (2023). Toward High-
267 Resolution Global Atmospheric Inverse Modeling Using Graphics Accelerators. *Geophysical
268 Research Letters*, 50(5), e2022GL102135. <https://doi.org/10.1029/2022GL102135>
- 269 Crowell, S., Baker, D., Schuh, A., Basu, S., Jacobson, A. R., Chevallier, F., Liu, J., Deng, F.,
270 Feng, L., McKain, K., Chatterjee, A., Miller, J. B., Stephens, B. B., Eldering, A., Crisp, D.,
271 Schimel, D., Nassar, R., O'Dell, C. W., Oda, T., ... Jones, D. B. A. (2019). The 2015–2016
272 carbon cycle as seen from OCO-2 and the global in situ network. *Atmospheric Chemistry and
273 Physics*, 19(15), 9797–9831. <https://doi.org/10.5194/acp-19-9797-2019>
- 274 Cui, Y. Y., Zhang, L., Jacobson, A. R., Johnson, M. S., Philip, S., Baker, D., Chevallier, F.,
275 Schuh, A. E., Liu, J., Crowell, S., Peiro, H. E., Deng, F., Basu, S., & Davis, K. J. (2022).
276 Evaluating Global Atmospheric Inversions of Terrestrial Net Ecosystem Exchange CO₂ Over
277 North America on Seasonal and Sub-Continental Scales. *Geophysical Research Letters*,
278 49(18). <https://doi.org/10.1029/2022GL100147>
- 279 Deng, Z., Ciais, P., Tzompa-Sosa, Z. A., Saunio, M., Qiu, C., Tan, C., Sun, T., Ke, P., Cui, Y.,
280 Tanaka, K., Lin, X., Thompson, R. L., Tian, H., Yao, Y., Huang, Y., Lauerwald, R., Jain, A.
281 K., Xu, X., Bastos, A., ... Chevallier, F. (2022). Comparing national greenhouse gas budgets
282 reported in UNFCCC inventories against atmospheric inversions. *Earth System Science Data*,
283 14(4), 1639–1675. <https://doi.org/10.5194/essd-14-1639-2022>
- 284 Friedlingstein, P., Jones, M. W., O'Sullivan, M., Andrew, R. M., Bakker, D. C. E., Hauck, J., Le
285 Quéré, C., Peters, G. P., Peters, W., Pongratz, J., Sitch, S., Canadell, J. G., Ciais, P., Jackson,
286 R. B., Alin, S. R., Anthoni, P., Bates, N. R., Becker, M., Bellouin, N., ... Zeng, J. (2022).
287 Global Carbon Budget 2021. *Earth System Science Data*, 14(4), 1917–2005.
288 <https://doi.org/10.5194/essd-14-1917-2022>
- 289 Fu, Y., Liao, H., Tian, X., Gao, H., Jia, B., & Han, R. (2021). Impact of Prior Terrestrial Carbon
290 Fluxes on Simulations of Atmospheric CO₂ Concentrations. *Journal of Geophysical
291 Research: Atmospheres*, 126(18). <https://doi.org/10.1029/2021JD034794>
- 292 Gelaro, R., McCarty, W., Suárez, M. J., Todling, R., Molod, A., Takacs, L., Randles, C. A.,
293 Darmenov, A., Bosilovich, M. G., Reichle, R., Wargan, K., Coy, L., Cullather, R., Draper, C.,
294 Akella, S., Buchard, V., Conaty, A., da Silva, A. M., Gu, W., ... Zhao, B. (2017). The
295 Modern-Era Retrospective Analysis for Research and Applications, Version 2 (MERRA-2).
296 *Journal of Climate*, 30(14), 5419–5454. <https://doi.org/10.1175/JCLI-D-16-0758.1>
- 297 Haynes, K. D., Baker, I. T., Denning, A. S., Stöckli, R., Schaefer, K., Lokupitiya, E. Y., &
298 Haynes, J. M. (2019). Representing Grasslands Using Dynamic Prognostic Phenology Based
299 on Biological Growth Stages: 1. Implementation in the Simple Biosphere Model (SiB4).

- 300 *Journal of Advances in Modeling Earth Systems*, 11(12), 4423–4439.
301 <https://doi.org/10.1029/2018MS001540>
- 302 Jiang, F., He, W., Ju, W., Wang, H., Wu, M., Wang, J., Feng, S., Zhang, L., & Chen, J. M.
303 (2022). The status of carbon neutrality of the world's top 5 CO₂ emitters as seen by carbon
304 satellites. *Fundamental Research*, 2(3), 357–366. <https://doi.org/10.1016/j.fmre.2022.02.001>
- 305 Kaiser, J. W., Heil, A., Andreae, M. O., Benedetti, A., Chubarova, N., Jones, L., Morcrette, J.-J.,
306 Razinger, M., Schultz, M. G., Suttie, M., & van der Werf, G. R. (2012). Biomass burning
307 emissions estimated with a global fire assimilation system based on observed fire radiative
308 power. *Biogeosciences*, 9(1), 527–554. <https://doi.org/10.5194/bg-9-527-2012>
- 309 Kuhlmann, G., Brunner, D., Broquet, G., & Meijer, Y. (2020). Quantifying CO₂ emissions of a
310 city with the Copernicus Anthropogenic CO₂ Monitoring satellite mission. *Atmospheric
311 Measurement Techniques*, 13(12), 6733–6754. <https://doi.org/10.5194/amt-13-6733-2020>
- 312 Liu, J., Fung, I., Kalnay, E., & Kang, J.-S. (2011). CO₂ transport uncertainties from the
313 uncertainties in meteorological fields. *Geophysical Research Letters*, 38, L12808.
314 <https://doi.org/10.1029/2011GL047213>
- 315 Liu, Z., Zeng, N., Liu, Y., Kalnay, E., Asrar, G., Cai, Q., & Han, P. (2023). *Assimilating the
316 dynamic spatial gradient of a bottom-up carbon flux estimation as a unique observation in
317 COLA (v2.0)*. <https://doi.org/10.5194/gmd-2023-15>
- 318 Liu, Z., Zeng, N., Liu, Y., Kalnay, E., Asrar, G., Wu, B., Cai, Q., Liu, D., & Han, P. (2022).
319 Improving the joint estimation of CO₂ and surface carbon fluxes using a constrained ensemble
320 Kalman filter in COLA (v1.0). *Geosci. Model Dev.*, 15, 5511–5528.
321 <https://doi.org/10.5194/gmd-15-5511-2022>
- 322 Martin, R. V., Eastham, S. D., Bindle, L., Lundgren, E. W., Clune, T. L., Keller, C. A., Downs,
323 W., Zhang, D., Lucchesi, R. A., Sulprizio, M. P., Yantosca, R. M., Li, Y., Estrada, L., Putman,
324 W. M., Auer, B. M., Trayanov, A. L., Pawson, S., & Jacob, D. J. (2022). Improved advection,
325 resolution, performance, and community access in the new generation (version 13) of the
326 high-performance GEOS-Chem global atmospheric chemistry model (GCHP). *Geoscientific
327 Model Development*, 15(23), 8731–8748. <https://doi.org/10.5194/gmd-15-8731-2022>
- 328 Oda, T., Maksyutov, S., & Andres, R. J. (2018). The Open-source Data Inventory for
329 Anthropogenic CO₂, version 2016 (ODIAC2016): A global monthly fossil fuel CO₂ gridded
330 emissions data product for tracer transport simulations and surface flux inversions. *Earth
331 System Science Data*, 10(1), 87–107. <https://doi.org/10.5194/essd-10-87-2018>
- 332 O'Dell, C. W., Eldering, A., Wennberg, P. O., Crisp, D., Gunson, M. R., Fisher, B.,
333 Frankenberg, C., Kiel, M., Lindqvist, H., Mandrake, L., Merrelli, A., Natraj, V., Nelson, R. R.,
334 Osterman, G. B., Payne, V. H., Taylor, T. E., Wunch, D., Drouin, B. J., Oyafuso, F., ...
335 Velasco, V. A. (2018). Improved retrievals of carbon dioxide from Orbiting Carbon
336 Observatory-2 with the version 8 ACOS algorithm. *Atmospheric Measurement Techniques*,
337 11(12), 6539–6576. <https://doi.org/10.5194/amt-11-6539-2018>
- 338 Palmer, P. I., Feng, L., Baker, D., Chevallier, F., Bösch, H., & Somkuti, P. (2019). Net carbon
339 emissions from African biosphere dominate pan-tropical atmospheric CO₂ signal. *Nature
340 Communications*, 10(1), 3344. <https://doi.org/10.1038/s41467-019-11097-w>
- 341 Peiro, H., Crowell, S., Schuh, A., Baker, D. F., O'Dell, C., Jacobson, A. R., Chevallier, F., Liu,
342 J., Eldering, A., Crisp, D., Deng, F., Weir, B., Basu, S., Johnson, M. S., Philip, S., & Baker, I.
343 (2022). Four years of global carbon cycle observed from the Orbiting Carbon Observatory 2
344 (OCO-2) version 9 and in situ data and comparison to OCO-2 version 7. *Atmospheric
345 Chemistry and Physics*, 22(2), 1097–1130. <https://doi.org/10.5194/acp-22-1097-2022>

- 346 Peylin, P., Law, R. M., Gurney, K. R., Chevallier, F., Jacobson, A. R., Maki, T., Niwa, Y., Patra,
347 P. K., Peters, W., Rayner, P. J., Rödenbeck, C., van der Laan-Luijkx, I. T., & Zhang, X.
348 (2013). Global atmospheric carbon budget: Results from an ensemble of atmospheric
349 CO₂ inversions. *Biogeosciences*, *10*(10), 6699–6720.
350 <https://doi.org/10.5194/bg-10-6699-2013>
- 351 Philip, S., Johnson, M. S., Potter, C., Genovesse, V., Baker, D. F., Haynes, K. D., Henze, D. K.,
352 Liu, J., & Poulter, B. (2019). Prior biosphere model impact on global terrestrial CO₂ fluxes
353 estimated from OCO-2 retrievals. *Atmospheric Chemistry and Physics*, *19*(20), 13267–13287.
354 <https://doi.org/10.5194/acp-19-13267-2019>
- 355 Rödenbeck, C., Bakker, D. C. E., Metzl, N., Olsen, A., Sabine, C., Cassar, N., Reum, F.,
356 Keeling, R. F., & Heimann, M. (2014). Interannual sea–air CO₂ flux variability from an
357 observation-driven ocean mixed-layer scheme. *Biogeosciences*, *11*(17), 4599–4613.
358 <https://doi.org/10.5194/bg-11-4599-2014>
- 359 Schimel, D., Stephens, B. B., & Fisher, J. B. (2015). Effect of increasing CO₂ on the terrestrial
360 carbon cycle. *Proceedings of the National Academy of Sciences*, *112*(2), 436–441.
361 <https://doi.org/10.1073/pnas.1407302112>
- 362 Schuh, A. E., Byrne, B., Jacobson, A. R., Crowell, S. M. R., Deng, F., Baker, D. F., Johnson, M.
363 S., Philip, S., & Weir, B. (2022). On the role of atmospheric model transport uncertainty in
364 estimating the Chinese land carbon sink. *Nature*, *603*(7901), E13–E14.
365 <https://doi.org/10.1038/s41586-021-04258-9>
- 366 Schuh, A. E., & Jacobson, A. R. (2022). Uncertainty in Parameterized Convection Remains a
367 Key Obstacle for Estimating Surface Fluxes of Carbon Dioxide. *Atmospheric Chemistry and*
368 *Physics Discussion [Preprint]*. <https://doi.org/10.5194/acp-2022-616>
- 369 Schuh, A. E., Jacobson, A. R., Basu, S., Weir, B., Baker, D., Bowman, K., Chevallier, F.,
370 Crowell, S., Davis, K. J., Deng, F., Denning, S., Feng, L., Jones, D., Liu, J., & Palmer, P. I.
371 (2019). Quantifying the Impact of Atmospheric Transport Uncertainty on CO₂ Surface Flux
372 Estimates. *Global Biogeochemical Cycles*, *33*(4), 484–500.
373 <https://doi.org/10.1029/2018GB006086>
- 374 Stephens, B. B., Gurney, K. R., Tans, P. P., Sweeney, C., Peters, W., Bruhwiler, L., Ciais, P.,
375 Ramonet, M., Bousquet, P., Nakazawa, T., Aoki, S., Machida, T., Inoue, G., Vinnichenko, N.,
376 Lloyd, J., Jordan, A., Heimann, M., Shibistova, O., Langenfelds, R. L., ... Denning, A. S.
377 (2007). Weak Northern and Strong Tropical Land Carbon Uptake from Vertical Profiles of
378 Atmospheric CO₂. *Science*, *316*(5832), 1732–1735. <https://doi.org/10.1126/science.1137004>
- 379 The International GEOS-Chem User Community. (2021). *geoschem/GCClassic: GEOS-Chem*
380 *13.0.2* (13.0.2). Zenodo. <https://doi.org/10.5281/ZENODO.4681204>
- 381 Wang, J., Feng, L., Palmer, P. I., Liu, Y., Fang, S., Bösch, H., O'Dell, C. W., Tang, X., Yang,
382 D., Liu, L., & Xia, C. (2020). Large Chinese land carbon sink estimated from atmospheric
383 carbon dioxide data. *Nature*, *586*(7831), 720–723. <https://doi.org/10.1038/s41586-020-2849-9>
- 384 Weir, B., Oda, T., Ott, L. E., & Schmidt, G. A. (2022). Assessing progress toward the Paris
385 Climate Agreement from Space. *Environmental Research Letters*.
386 <https://doi.org/10.1088/1748-9326/ac998c>
- 387 Yu, K., Keller, C. A., Jacob, D. J., Molod, A. M., Eastham, S. D., & Long, M. S. (2018). Errors
388 and improvements in the use of archived meteorological data for chemical transport modeling:
389 An analysis using GEOS-Chem v11-01 driven by GEOS-5 meteorology. *Geoscientific Model*
390 *Development*, *11*(1), 305–319. <https://doi.org/10.5194/gmd-11-305-2018>

1 **Supporting Information for**

2 **"Large impact of coarse-resolution atmospheric transport model error on land-ocean**
3 **and tropic-extratropic partitioning and seasonal cycle in CO₂ inversion"**
4

5 **Zhiqiang Liu^{1,2}, Ning Zeng^{3,4}, Pengfei Han^{5,1}, Qixiang Cai¹**

6 ¹Laboratory of Numerical Modeling for Atmospheric Sciences & Geophysical Fluid Dynamics,
7 Institute of Atmospheric Physics, Chinese Academy of Sciences, Beijing, China

8 ²University of Chinese Academy of Sciences, Beijing, China

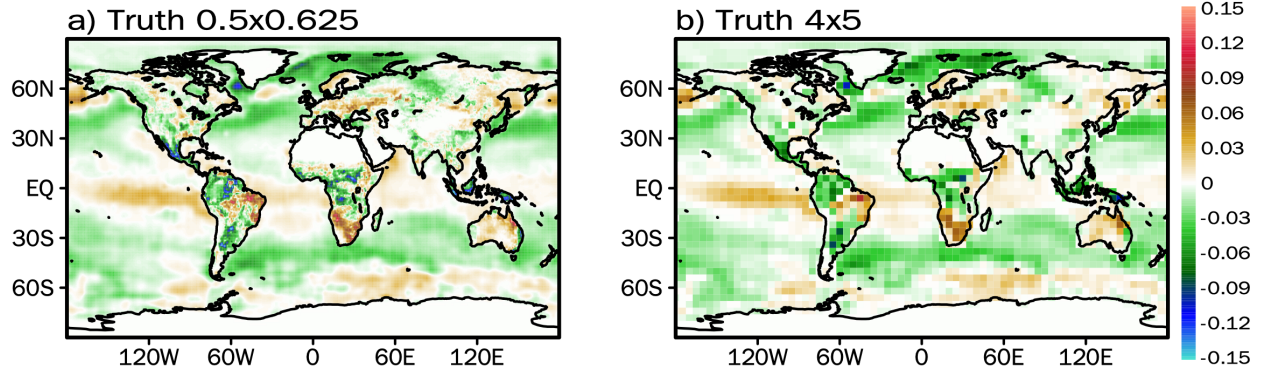
9 ³Dept. of Atmospheric and Oceanic Science, University of Maryland, USA

10 ⁴Earth System Science Interdisciplinary Center, University of Maryland, USA

11 ⁵Carbon Neutrality Research Center, Institute of Atmospheric Physics, Chinese Academy of
12 Sciences, Beijing, China

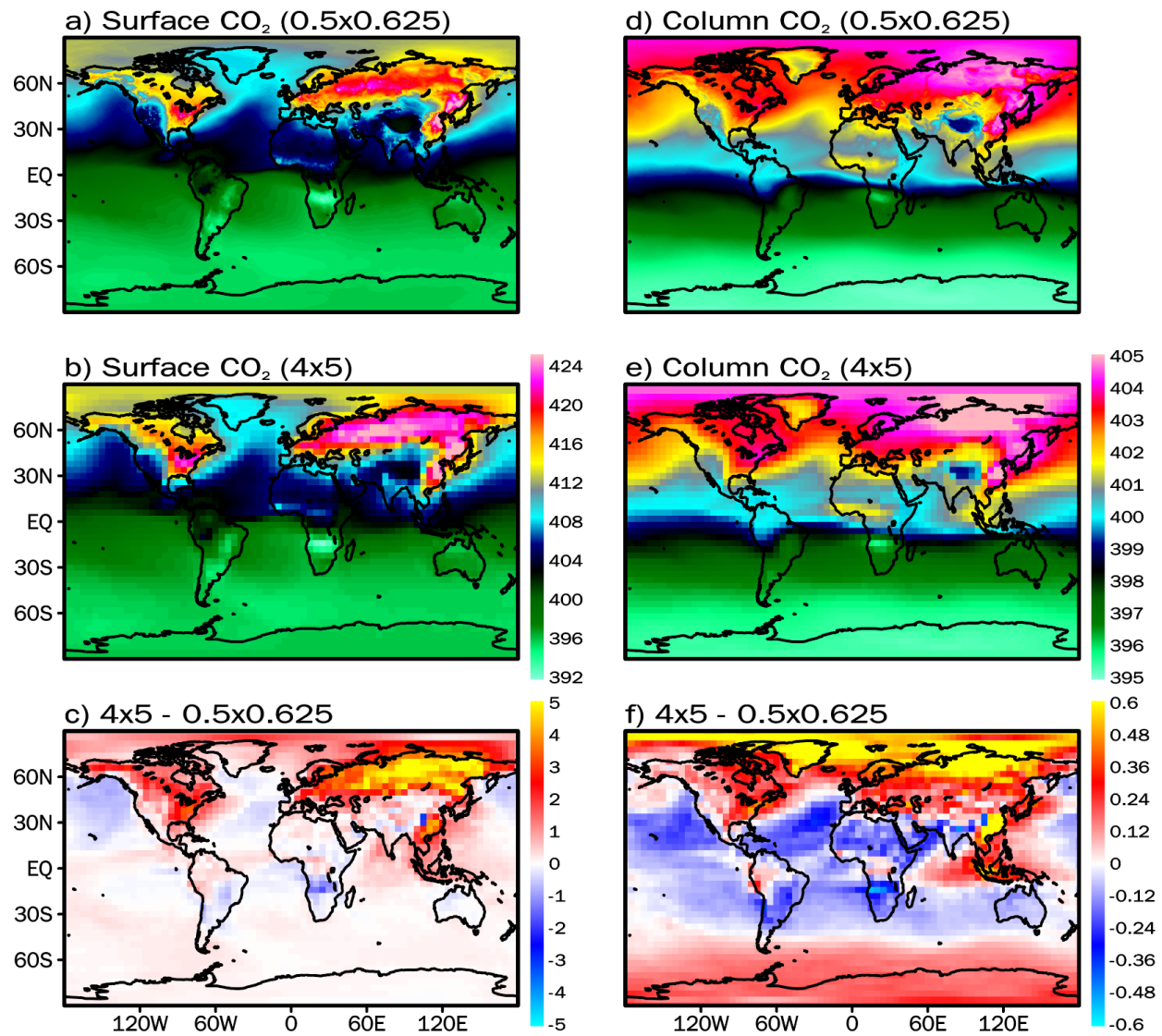
13
14 **Contents**

15 Figures S1 to S3
16
17
18
19
20
21
22
23
24
25
26
27
28
29
30
31
32
33
34
35
36
37
38
39
40
41
42



43
44
45

Figure S1. The annual mean true surface land and ocean fluxes in nature runs of (a) EXP-biased at $0.5^\circ \times 0.625^\circ$ resolution and (b) EXP-perfect at $4^\circ \times 5^\circ$ resolution.



46
47
48
49

Figure S2. The mean surface CO_2 and column CO_2 pattern of nature runs at horizontal resolutions of $0.5^\circ \times 0.625^\circ$ (a, d) and $4^\circ \times 5^\circ$ (b, e) from January to March. (c, f) The difference between the two nature runs.

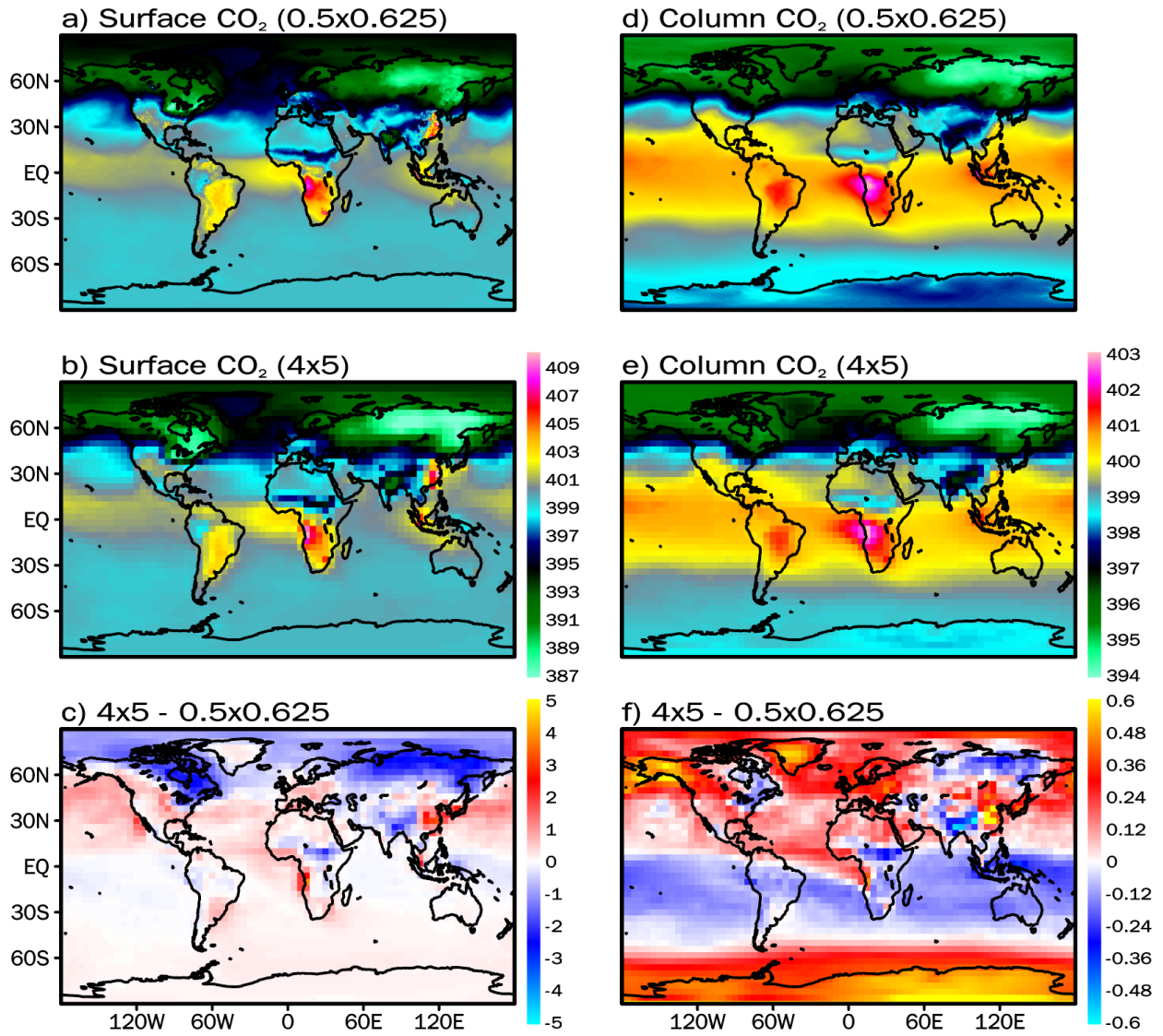


Figure S3. The mean surface CO₂ and column CO₂ pattern of nature runs at horizontal resolutions of 0.5° × 0.625° (a, d) and 4° × 5° (b, e) from July to September. (c, f) The difference between the two nature runs.

50
51
52
53
54
55